ETH zürich

ETH Library

Cadmium isotopes in chondrites and acid leachates: Nucleosynthetic homogeneity and a monitor for thermal neutron capture effects

Journal Article

Author(s):
Toth, Eniko R.; Fehr, Manuela A.; Friebel, Matthias; Schönbächler, Maria

Publication date:
2020-04

Permanent link:
https://doi.org/10.3929/ethz-b-000403157

Rights / license:
Creative Commons Attribution-NonCommercial-NoDerivatives 4.0 International

Originally published in:
Geochimica et Cosmochimica Acta 274, https://doi.org/10.1016/j.gca.2020.01.059

This page was generated automatically upon download from the ETH Zurich Research Collection.
For more information, please consult the Terms of use.

Available online at www.sciencedirect.com

ScienceDirect

Geochimica et Cosmochimica Acta 274 (2020) 286–301

Geochimica et Cosmochimica Acta

www.elsevier.com/locate/gca

Cadmium isotopes in chondrites and acid leachates: Nucleosynthetic homogeneity and a monitor for thermal neutron capture effects

Eniko R. Toth *, Manuela A. Fehr, Matthias Friebel, Maria Schönbächler

Institute of Geochemistry and Petrology, ETH Zürich, Clausiusstrasse 25, 8092 Zürich, Switzerland

Received 29 July 2019; accepted in revised form 31 January 2020; available online 6 February 2020

Abstract

Nucleosynthetic isotope variations are well documented for refractory elements in meteorites and the Earth, while moderately volatile elements generally display homogeneous compositions. Cadmium is a moderately volatile element with eight stable isotopes generated by a variety of nucleosynthetic processes. To address the extent of the nucleosynthetic variability in moderately volatile elements, new high precision Cd isotope data are presented for bulk samples of six carbonaceous and one enstatite chondrite. In addition, we report the first Cd isotope results of sequential acid leachates for the CM2 chondrite Jbilet Winselwan. Our new Cd data displays nucleosynthetic homogeneity for bulk chondrites and acid leachates within analytical uncertainties, in agreement with results for other moderately volatile elements. This implies that Cd isotopes were efficiently homogenised prior to incorporation into planetary bodies. We propose that Cd never significantly condensed into dust in stellar environments, or alternatively that such Cd-bearing dust was efficiently destroyed and recycled in the interstellar medium. Our leachate data provides evidence for further homogenisation during thermal processing in the protoplanetary disk including parent body processing. The data shows that Cd in carbonaceous chondrites mainly resides in the more easily dissolved phases, most likely sulphides that were affected by aqueous alteration. Less than 1% of the total Cd was recovered in the final leach fractions that employed HF and mainly dissolve silicates and refractory oxides.

Cadmium is susceptible to thermal neutron-capture effects due to the large neutron capture cross-section of ^{113}Cd (~20,000 barns). We report variations of up to -0.6 ± 0.3 for ε^{113}Cd (internally normalised to ^{116}Cd/^{111}Cd) in bulk chondrites, which renders Cd a potential thermal neutron-capture monitor. Most neutron dosimeters, such as Pt, Os and Hf, are sensitive to neutron capture in the epithermal energy range and have applications mainly limited to lunar samples or iron and stony-iron meteorites. The additional use of Cd, susceptible to neutron capture in the thermal energy range, therefore provides a new tool to determine the exposure histories of stony meteorites in more detail. Our study demonstrates that thermal neutron-capture effects in carbonaceous and enstatite chondrites can produce resolvable effects and require attention when assessing nucleosynthetic isotope variations.

© 2020 The Authors. Published by Elsevier Ltd. This is an open access article under the CC BY-NC-ND license (http://creativecommons.org/licenses/by-nc-nd/4.0/).

Keywords: Cd isotopes; Bulk chondrites; Sequential acid leachates; Nucleosynthesis; Thermal neutron-capture

1. INTRODUCTION

Nucleosynthetic isotope variations are well established for several refractory elements (elements with half-mass condensation temperatures (50% T_C) above ~1200–1300 K (Wood et al., 2019)) at the bulk rock scale in our

* Corresponding author.
E-mail address: eniko.toth@erdw.ethz.ch (E.R. Toth).

https://doi.org/10.1016/j.gca.2020.01.059
0016-7037/© 2020 The Authors. Published by Elsevier Ltd.
This is an open access article under the CC BY-NC-ND license (http://creativecommons.org/licenses/by-nc-nd/4.0/).

solar system, including Ca (Chen et al., 2011; Dauphas et al., 2014; Schiller et al., 2015), Ti (Leya et al., 2008; Trinquier et al., 2009; Zhang et al., 2012), Cr (Trinquier et al., 2007; Qin et al., 2010), Ni (Steele et al., 2012), Zr (Akram et al., 2015), Mo (Dauphas et al., 2004; Burkhardt et al., 2011), Ru (Chen et al., 2010; Fischer-Gödde et al., 2015), Ba (Andreasen and Sharma, 2007; Carlson et al., 2007) and Nd (Andreasen and Sharma, 2006; Carlson et al., 2007; Bouvier and Boyet, 2016; Burkhardt et al., 2016). On the other hand, moderately volatile elements (50% T_C of 1250–252 K (Palme et al., 2014)), such as Te, Se and Zn with a 50% T_C of 709–665 K, 701–697 K and 726–704 K, respectively (Lodders, 2003; Wood et al., 2019), display no resolved nucleosynthetic isotope variations in bulk chondrites (Fehr et al., 2005; Moynier et al., 2009; Labidi et al., 2018). Several solutions for this apparent dichotomy between the refractory and the moderately volatile elements have been put forward. It has been proposed that moderately volatile elements lack resolvable isotope anomalies because of their volatile nature, having experienced efficient homogenisation through thermal processing prior to incorporation into their respective parent bodies. This may include thermal processing events in the solar nebula or even before solar system formation in their stellar nucleosynthetic formation environment (e.g. Fehr et al., 2006). Due to their volatile nature, moderately volatile elements preferentially partition into the gas phase during thermal processing, where diffusion time scales are much faster and allow for rapid mixing and homogenisation of the isotopic compositions. To better constrain the origin of the dichotomy between refractory and moderately volatile elements, Cd isotopes are a promising tool. Cadmium is a moderately volatile element with a 50% T_C of 652–502 K, similar to that of Te, Se and Zn (Lodders, 2003; Wood et al., 2019). It has eight stable isotopes produced by different nucleosynthetic processes: ^{106}Cd and ^{108}Cd by the *p*-process, ^{110}Cd dominantly by the *s*-process, and ^{111}Cd to ^{116}Cd by a combination of the *s*- and the *r*-process in different proportions (Bisterzo et al., 2011; and references therein). Cadmium is therefore a prime candidate to further constrain nucleosynthetic isotope variations.

Nucleosynthetic anomalies provide strong evidence that a variety of stellar sources contributed material to our nascent solar system, such as AGB stars and supernovae (e.g. Steele et al., 2012; Akram et al., 2015). They are generated by the heterogeneous distribution of nm- to μm-sized presolar grains in the protoplanetary disk. These grains condensed in various stellar environments and preserved the extreme isotopic compositions of their formation site (Zinner, 2014). The heterogeneous distribution of these grains in the protoplanetary disk was sampled and preserved by planetesimals and planets. The process(es) that generated the heterogeneous distribution are still debated. Chondrites and achondrites, as well as martian and terrestrial samples, exhibit well defined linear correlations between nucleosynthetic variations in Zr, Mo, Ru, and Pd (e.g. Dauphas et al., 2004; Chen et al., 2010; Burkhardt et al., 2011; Akram et al., 2015; Fischer-Gödde et al., 2015; Poole et al., 2017; Ek et al., 2020), which are generally attributed to a depletion of *s*-process material in carbonaceous chondrites relative to the Earth. At the same time, Ca, Ti, Cr and Ni display excesses of supernova material in carbonaceous chondrites (Trinquier et al., 2007; Leya et al., 2008; Trinquier et al., 2009; Chen et al., 2011; Steele et al., 2012; Schiller et al., 2015), whereas heavy elements (e.g. Os and Pt) generally show nucleosynthetic homogeneity (Yokoyama et al., 2010; Hunt et al., 2017), with a few exceptions such as Os isotopes in a few ureilites (Goderis et al., 2015).

To explain the correlated heterogeneities, physical and/or chemical processing of carrier phases must have occurred in the solar protoplanetary disk and played a vital role in preserving selected isotope anomalies (e.g. Regelous et al., 2008; Trinquier et al., 2009; Akram et al., 2015). Such processes include selective size sorting of dust grains (e.g. Regelous et al., 2008; Dauphas et al., 2010) and thermal processing of more-labile carrier phases (Trinquier et al., 2009; Burkhardt et al., 2011; Akram et al., 2015). Alternatively, some of the nucleosynthetic variations may be inherited from the molecular cloud, from which our solar system formed (Van Kooten et al., 2016; Nanne et al., 2019). Ek et al. (2020) proposed that the subdued nucleosynthetic effects in Pd compared to those in the refractory elements Zr, Mo and Ru stem from the more volatile nature of Pd (50% T_C = 1330–1324 K; Lodders, 2003; Wood et al., 2019). This implies that Pd was incorporated to a lesser extent into the presolar grains (also called stardust) around AGB stars, which contributed most presolar grains to the solar system that carry an *s*-process signature. Since Cd isotopes are similar in mass to Pd (and Zr, Mo, Ru) isotopes, Cd should also carry *s*-process isotope variations (Ek et al., 2020). However, in the framework of the Ek et al. (2020) model, Cd is expected to condense even less than Pd into refractory presolar grains around AGB stars because Cd is significantly more volatile (e.g. Lodders and Fegley, 1997). If correct, high precision Cd isotope data would reflect this interpretation by showing no evidence of nucleosynthetic isotope variations.

Critical to the determination of nucleosynthetic Cd isotope variability in the solar system is the appropriate consideration of thermal neutron capture effects that can also create mass-independent Cd isotope variations in meteorites. While in space, meteorites are exposed to galactic cosmic-rays (GCR) composed of mostly energetic protons and some alpha particles (Masarik, 1997). As the meteorite's surface interacts with GCR, secondary neutrons are liberated that lead to further reactions deeper inside the body (Leya and Masarik, 2013). Cadmium is particularly susceptible to the capture of such secondary neutrons in the thermal energy range (~0.025 eV) due to the large neutron capture cross-section of ^{113}Cd (~20,000 barns) (e.g. Leya and Masarik, 2013). This can lead to the consumption of ^{113}Cd and the corresponding production of ^{114}Cd (^{113}Cd (n,γ) ^{114}Cd). Depending on the radius, shielding depth and the cosmic-ray exposure (CRE) age of the meteorite, carbonaceous chondrites may show variations of up to −0.6 in ε^{113}Cd (internally normalised to ^{116}Cd/^{111}Cd) per Ma exposure (Leya and Masarik, 2013). Moreover, large GCR effects on ^{113}Cd are well documented for lunar

samples with long exposure to GCR on the lunar surface (Sands et al., 2001; Wombacher et al., 2008). This suggests that Cd may be an ideal neutron capture monitor for samples with sufficient Cd, where high precision Cd isotope analysis is possible.

Neutron capture monitors are essential because neutron capture reactions can disturb the isotope systematics of short-lived nuclides used as early solar system chronometers, including ^{182}Hf-^{182}W, ^{53}Mn-^{53}Cr and ^{107}Pd-^{107}Ag (e.g. Leya et al., 2003; Schönbächler et al., 2008; Sprung et al., 2010; Leya and Masarik, 2013; Hunt et al., 2018). Elements such as Pt and Os (e.g. Kruijer et al., 2013; Wittig et al., 2013; Hunt et al., 2017) are more susceptible to neutron capture in the epithermal energy range (1–10 keV; Leya and Masarik, 2013) and have been used as neutron dose proxies for iron-rich meteorites. In stony meteorites, thermal neutron capture effects dominate (energy range of 0.025 eV; Leya and Masarik, 2013) and only Sm and Gd were used as dosimeters so far (e.g. Eugster et al., 1970; Hidaka et al., 2000; Sprung et al., 2010). Cadmium has been studied as a potential neutron dose proxy for iron meteorites, but because of its very low concentration and lack of epithermal neutron capture effects, it was considered unsuitable (Kruijer et al., 2013). However, Cd is more abundant in chondrites where thermal neutron capture dominates. Furthermore, in carbonaceous chondrites secondary neutrons are more efficiently thermalised because they lose energy more quickly during collisions with hydrogen (water) (Leya and Masarik, 2013). Therefore, Cd might serve as an ideal thermal neutron capture monitor for primitive meteorites.

Previous studies reported no evidence for nucleosynthetic or thermal neutron capture induced Cd isotope variations in bulk meteorites, within analytical uncertainties of ±4.3 ε (2 standard deviations, SD) for ^{114}Cd/^{110}Cd and of ±1.3 ε for ^{113}Cd/^{114}Cd (Wombacher et al., 2003; Wombacher et al., 2008). However, thermal neutron capture effects on Cd are predicted to be small, likely in the sub-epsilon range (Leya and Masarik, 2013). Therefore, it is important to reinvestigate the Cd isotope composition of bulk chondrites and terrestrial samples at a higher precision, to examine whether nucleosynthetic anomalies and neutron capture effects are absent for Cd, or if they were simply unresolvable in previous studies due to analytical constraints. To address these issues, we present new high-precision Cd isotope data for three terrestrial sediments, six carbonaceous and one enstatite chondrite. Additionally, we report the first Cd isotope data of a leaching experiment derived from the sequential digestion of the CM2 chondrite Jbilet Winselwan.

2. SAMPLES AND ANALYTICAL PROCEDURE

2.1. Sample materials

Powdered bulk samples of the chondrites Allende (CV3), Murchison (CM2), Jbilet Winselwan (CM2), Miller Range (MIL) 090001 (CR2), Elephant Moraine (EET) 92048 (CR2), Graves Nunataks (GRA) 06100 (CR2) and Indarch (EH4) were analysed in this study. Furthermore, a ~1.5 g powdered aliquot of Jbilet Winselwan (CM2) was used for a leach experiment. The accuracy and precision of the employed analytical procedure was tested by analysing a sediment core sample from Lake Zürich (Lake Zürich I also called ZH09-05, sample depth 23.3–24 cm, ~14 ppm Cd) (Friebel et al., 2020) and the Cd-rich USGS Fe-Mn nodules Nod-A-1 (6.81 ppm Cd) and Nod-P-1 (20.9 ppm Cd) (Horner et al., 2010).

2.2. Digestion procedures

About 1 g of powdered meteorite (~0.8 g of Indarch) was digested in Parr® bomb vessels in ~200 mg fractions for 4½ days at 170 °C in an oven using 0.7 ml concentrated (conc.) HNO_3 and 3 ml conc. HF. Each sample fraction was then evaporated to dryness and re-dissolved in 5 ml 6 M HCl for a day on a hot plate at 80–100 °C. The five separate fractions were then combined for each meteorite and dried down again. This procedure results in a complete dissolution of the samples yielding a clear solution in 6 M HCl. For Indarch, a further overnight digestion step using 4 ml aqua regia ($HCl:HNO_3 = 3:1$) at 80 °C was employed to dissolve organic components.

For comparison, a second fraction of Allende was dissolved using a hotplate digestion procedure. This involved sample dissolution in 7 ml conc. HNO_3 and 15 ml conc. HF for 2 days, and the successive overnight digestions with 25 ml 6 M HNO_3, 20 ml aqua regia ($HCl:HNO_3 = 3:1$) and 20 ml 6 M HCl. At this stage, the sample solution was centrifuged, the supernatant decanted and the remaining residue further treated with 20 ml 6 M HCl overnight. The sample solution and the supernatant were then combined and fully dried down.

A ~0.1 g powdered fraction of the lake sediment was digested using the hotplate procedure outlined in Friebel et al. (2020). Another ~0.1 g aliquot was also digested using the Parr® bomb method to test whether the digestion procedures influence the accuracy of the data. The Fe-Mn nodules were processed in ~0.1 g fractions and digested overnight on a hotplate in 10 ml 6 M HCl at 100 °C following the procedure described by Horner et al. (2010).

The carbonaceous chondrite Jbilet Winselwan was leached using a similar procedure (Table 1) as in previous studies (Schönbächler et al., 2003; Schönbächler et al., 2005; Fehr et al., 2006). Our leaching experiment was adjusted for the joint study of Cd and Sn isotopes (Friebel et al., 2020) based on published Te and Sn concen-

Table 1
Leach procedure of Jbilet Winselwan.

Step	Reagent	Procedure
1b	50% HAc	1 day, RT
2a	1 M HNO_3	1 h, RT
2b	4 M HNO_3	5 days, RT
3a	6 M HCl	5 days, RT
3b + c	6 M HCl	1 day, 80 °C
4	13.5 M HF + 3 M HCl	4 days, 100 °C
5	conc. HF + HNO_3	4 days, 170 °C, Parr® bomb

RT: Room Temperature; HAc: CH_3COOH.

tration data of the CM2 chondrite Murchison (Fehr et al., 2006). Specifically, we omitted the first 2.5% HAc and the second 6 M HCl steps, and added an additional 1 M HNO_3 leaching stage. This was done to further target sulphur-bearing minerals that are leached by HNO_3, because they may host significant amounts of Cd in carbonaceous chondrites based on the Te concentration data (Fehr et al., 2006). This generated a total of 7 leach fractions. After each leach step, the sample was centrifuged, the supernatant decanted and the remaining residue treated with the next acid.

2.3. Chemical separation

To separate Cd from the rock matrix, a four-stage chromatographic separation procedure was employed, as detailed in Friebel et al. (2020). It represents a combination of the procedures developed for the separation of Sn (Friebel et al., 2020) and Cd (Wombacher et al., 2003) using the AG 1-X8 anion-exchange, Eichrom TRU and Pre-filter resins. Samples of up to 1 g were loaded on one column. Tin isotope data of the investigated samples are reported in a parallel study (Friebel, 2018; Friebel et al., 2020), focusing on the investigation of nucleosynthetic isotope variations of the moderately volatile element Sn (50% T_C of 704–604 K) (Lodders, 2003; Wood et al., 2019).

2.4. Mass spectrometry

Cadmium isotope measurements were performed with a Nu Plasma II multiple collector inductively coupled plasma mass spectrometer (MC-ICPMS) at ETH Zürich, as outlined in Friebel et al. (2020). All samples were dissolved in 0.5 M HNO_3 prior to analysis. They were introduced to the plasma using a DSN-100 desolvating nebuliser system in combination with a PFA nebuliser (flow-rate ~50–60 µl/min). Palladium, In and Sn can generate direct isobaric interferences onto Cd isotopes. To allow for their correction, two measurement cycles were used. The first cycle included all Cd isotopes, ^{115}In and ^{118}Sn, while the second one ^{105}Pd, ^{108}Cd, as well as ^{111}Cd for drift correction. Each analysis comprised an initial peak centre for both cycles and the measurement of an electronic baseline for 30 s with the ion beam deflected by the electrostatic analyser. This was then followed by 30 dynamic isotope measurements with a 2 s magnet delay time, using 10 s (first cycle) and 5 s (second cycle) integrations. One full analysis lasted ~12 min consuming ~100–150 ng Cd for 200 ppb Cd solutions. For the low concentration analyses (at 3.4, 2.3 and 1 ppb Cd consuming ~2.0, ~1.3 and ~0.6 ng Cd, respectively) of terrestrial samples, leachates and meteorites, the peak centre routine was omitted to minimise the amount of solution required.

Isotope measurements were performed at 200 ppb Cd concentrations, except for those samples with lower Cd contents where this was not possible (GRA 06100, leach 3a, 3b + c, 4 and 5). At this concentration, an average total ion beam intensity of 2.05×10^{-9} A/ppm Cd was achieved using 10^{11} Ω resistors. Each sample analysis was bracketed by measurements of an Alfa Aesar Cd standard solution with a matching concentration on average to within ±20%. Various Cd concentrations (100 ppb, 200 ppb, 250 ppb, 300 ppb and 400 ppb Cd) and measurement lengths (20 to 40 integrations) were tested when establishing the method (Table S1). The results show that using 200 ppb Cd and 30 integrations is most suitable for high precision and reliable measurement including the low abundance isotopes ^{108}Cd and ^{106}Cd, considering the available sample amount and Cd content of chondrites.

On-peak measurements in 0.5 M HNO_3 used for background correction were collected every three standard and/or sample analyses. This correction was necessary for the accurate determination of the low abundance Cd isotopes. To correct for mass-dependent fractionation, Cd isotope data were internally normalised to $^{116}Cd/^{111}Cd = 0.578505$ (Wombacher et al., 2004), which is not affected by thermal neutron capture effects, using the exponential law. Furthermore, this isotope pair covers a large mass range, utilises the only Cd isotope (^{111}Cd) free of isobaric interferences in conjunction with one of similar nucleosynthetic production (^{116}Cd), and allows nucleosynthetic and cosmogenic effects to be easily distinguished (Friebel et al., 2020). Results are given in the epsilon notation and were calculated using the standard-sample bracketing method relative to an Alfa Aesar Cd standard: $\varepsilon^{i}Cd = \{[(^{i}Cd/^{111}Cd)_{sample}/(^{i}Cd/^{111}Cd)_{standard}] - 1\} \times 10^{4}$, where i refers to the mass of the isotope of interest. Additionally, the data was internally normalised using $^{112}Cd/^{114}Cd$, $^{110}Cd/^{114}Cd$ and $^{113}Cd/^{111}Cd$ for further data evaluation.

Using a 200 ppb Alfa Aesar Cd standard solution, the average reproducibility (2SD) achieved per measurement day (n = 40) and corrected for drifts in the isotope ratios (Friebel et al., 2020) was 0.96 for ε^{106}Cd, 1.13 for ε^{108}Cd, 0.28 for ε^{110}Cd, 0.16 for ε^{112}Cd, 0.20 for ε^{113}Cd and 0.17 for ε^{114}Cd (Table 2 and Friebel et al., 2020). The external reproducibility estimated from repeated analyses of Nod-P-1 (2SD, n = 25) yields very similar uncertainties of 1.25 for ε^{106}Cd, 1.08 for ε^{108}Cd, 0.36 for ε^{110}Cd, 0.23 for ε^{112}Cd, 0.27 for ε^{113}Cd and 0.24 for ε^{114}Cd (Table 2).

2.5. Influence of sample purity after Cd purification on accuracy and precision

The final Cd content of each sample was checked on the Nu Plasma II MC-ICPMS prior to isotope analysis using a 2–5% sample aliquot. This solution was monitored for potential interfering elements by performing peak scans in their mass ranges (“mass-scans”). All meteorite and leachate samples measured at 200 ppb Cd generally had impurities (of Zn, Zr, Mo, Pd, In and Sn) below their determined tolerance thresholds (Friebel et al., 2020). A previous study demonstrated the effects of organics on high-precision Cd isotope analyses (Gault-Ringold and Stirling, 2012). The authors identified large offsets for pure Cd standards doped with aliquots of organic residue eluted from the TRU resin. They concluded that organics, most likely P derived from the resin beads, were responsible for the observed offsets. Phosphorus can generate resolvable molecular interferences onto Cd isotopes ($^{31}P + ^{40}Ar + ^{40}Ar \rightarrow ^{111}Cd$), if present in large quantities, but also matrix effects that are more diffi-

Table 2
Cadmium isotope data of terrestrial standards, samples, bulk chondrites and acid leachates of Jbilet Winselwan.

Sample		Cd ppb	Cd ng	% of total Cd eluted	Yield (%)	Blank (%)	$^{118}Sn/^{111}Cd$	$^{115}In/^{111}Cd$	$^{105}Pd/^{111}Cd$	N	$\varepsilon^{106}Cd$	$\varepsilon^{108}Cd$	$\varepsilon^{110}Cd$	$\varepsilon^{112}Cd$	$\varepsilon^{113}Cd$	$\varepsilon^{114}Cd$
Terrestrial standards																
Alfa Aesar Cd standard		200[#]								40*	0.00 ± 0.96	0.00 ± 1.13	0.00 ± 0.28	0.00 ± 0.16	0.00 ± 0.20	0.00 ± 0.17
		33								10*	0.02 ± 3.20	−0.05 ± 4.88	−0.01 ± 0.56	−0.01 ± 0.30	−0.01 ± 0.33	−0.01 ± 0.43
		16.5								13	−0.02 ± 8.59	0.5 ± 12.9	0.05 ± 0.33	−0.01 ± 0.44	0.03 ± 0.63	0.00 ± 0.55
		3.4								4*	−0.6 ± 35.3	−0.3 ± 47.7	−0.02 ± 3.61	−0.01 ± 2.16	0.03 ± 2.61	0.02 ± 2.80
		2.3								4*	−0.3 ± 51.7	0.2 ± 61.8	−0.03 ± 5.59	−0.10 ± 3.91	−0.05 ± 5.83	−0.01 ± 4.33
		1								2*	3 ± 135	3 ± 201	0.0 ± 10.2	−0.02 ± 5.63	−0.06 ± 7.78	0.04 ± 8.36
NIST SRM 3108 Cd		33								15	0.39 ± 3.41	0.43 ± 3.70	0.06 ± 0.59	−0.01 ± 0.36	−0.09 ± 0.30	0.01 ± 0.42
Column processed standards																
Alfa Aesar Cd standard		200[#]								9	1.04 ± 3.50	0.48 ± 2.90	0.15 ± 0.33	0.11 ± 0.21	−0.02 ± 0.15	0.03 ± 0.24
Cd-Zn standard		200[#]								4	0.69 ± 1.17	−0.19 ± 0.55	−0.03 ± 0.24	0.01 ± 0.11	−0.07 ± 0.19	−0.04 ± 0.10
Terrestrial Samples																
Lake Zürich I Sediment HP		200[#]								6	0.37 ± 1.56	0.05 ± 2.14	0.13 ± 0.27	0.07 ± 0.18	−0.07 ± 0.22	0.00 ± 0.16
		3.4								1	10.2 ± 47.1	−33.1 ± 65.1	−0.35 ± 4.48	2.06 ± 2.88	−0.53 ± 1.95	0.11 ± 3.15
		2.3								3	35.1 ± 72.1	36.7 ± 38.9	3.90 ± 4.97	1.70 ± 0.49	−1.32 ± 1.76	0.26 ± 2.03
		1								1	−57 ± 162	−1 ± 220	−3.64 ± 9.19	3.32 ± 6.96	4.15 ± 7.55	−0.52 ± 8.38
Lake Zürich I Sediment PB		200[#]								3	−0.13 ± 1.95	−0.21 ± 2.21	0.05 ± 0.51	0.03 ± 0.20	−0.16 ± 0.28	−0.02 ± 0.15
		2.3								2	22.8 ± 61.8	22.4 ± 12.9	4.00 ± 1.11	2.85 ± 1.37	2.28 ± 0.27	2.63 ± 1.28
Nod-P-1		200								25	0.00 ± 1.25	−0.22 ± 1.08	0.15 ± 0.36	0.09 ± 0.23	−0.06 ± 0.27	0.03 ± 0.24
		3.4								12	−3.9 ± 37.8	−7.0 ± 43.9	0.44 ± 3.65	0.80 ± 2.32	−0.54 ± 2.52	0.90 ± 1.91
		2.3								1	−15.7 ± 63.0	−66.8 ± 55.6	2.05 ± 7.59	3.44 ± 3.70	−1.72 ± 6.26	0.48 ± 2.93
		1								1	27 ± 162	70 ± 220	3.44 ± 9.19	2.88 ± 6.96	5.35 ± 7.55	1.61 ± 8.38
Nod-A-1		200								4	−0.29 ± 0.99	−0.54 ± 0.67	0.08 ± 0.41	0.06 ± 0.17	−0.08 ± 0.34	0.03 ± 0.16
Bulk meteorites																
Jbilet Winselwan	CM2	200					1.1E−04	1.3E−05	3.7E−05	1	−0.02 ± 0.78	0.00 ± 1.24	0.03 ± 0.27	−0.05 ± 0.14	−0.59 ± 0.15	0.21 ± 0.11
	CM2	200					3.1E−04	1.0E−05	2.1E−05	1	−0.04 ± 0.74	0.19 ± 1.00	0.09 ± 0.28	0.02 ± 0.20	−0.66 ± 0.26	0.28 ± 0.24
	CM2	200					2.1E−04	8.4E−06	3.3E−05	1	−0.89 ± 0.94	−0.75 ± 1.30	0.10 ± 0.22	0.18 ± 0.12	−0.42 ± 0.24	0.37 ± 0.25
Jbilet Winselwan Mean	CM2	200	355		83	0.02				3	−0.32 ± 1.25[†]	−0.19 ± 1.08[†]	0.07 ± 0.36[†]	0.05 ± 0.24	−0.56 ± 0.27[†]	0.29 ± 0.24[†]
Murchison	CM2	200					2.8E−04	8.3E−06	2.0E−05	1	0.75 ± 0.74	0.27 ± 1.00	−0.08 ± 0.28	0.01 ± 0.20	−0.25 ± 0.26	0.00 ± 0.24
	CM2	200					2.7E−04	1.7E−05	2.6E−05	1	0.09 ± 0.94	−0.28 ± 1.37	−0.07 ± 0.27	0.01 ± 0.13	−0.24 ± 0.18	−0.11 ± 0.17
	CM2	200					1.4E−04	2.4E−06	2.5E−05	1	0.68 ± 0.78	1.08 ± 0.93	−0.01 ± 0.16	−0.03 ± 0.13	−0.21 ± 0.18	0.04 ± 0.15
Murchison Mean	CM2	200	314		80	0.03				3	0.51 ± 1.25[†]	0.36 ± 1.37	−0.06 ± 0.36[†]	0.00 ± 0.23[†]	−0.23 ± 0.27[†]	−0.02 ± 0.24[†]
Allende HP	CV3	200	162		75	0.07	1.6E−04	1.1E−05	4.5E−05	1	−0.48 ± 1.07	−0.59 ± 1.06	−0.25 ± 0.26	−0.22 ± 0.15	−0.46 ± 0.14	−0.16 ± 0.15
Allende PB	CV3	200	172		74	0.14	2.1E−04	1.0E−05	3.1E−05	1	−1.21 ± 0.75	−1.81 ± 1.23	−0.31 ± 0.28	−0.20 ± 0.15	−0.31 ± 0.18	−0.01 ± 0.15
	CV3	200					2.0E−04	1.2E−05	2.6E−05	1	0.42 ± 0.94	−0.36 ± 1.37	−0.04 ± 0.27	−0.07 ± 0.13	−0.26 ± 0.18	0.06 ± 0.17
	CV3	200	200		84	0.01	1.6E−04	6.9E−06	2.2E−05	1	0.71 ± 0.78	0.39 ± 0.93	−0.16 ± 0.16	−0.02 ± 0.13	−0.50 ± 0.18	−0.15 ± 0.15

(*continued next page*)

Table 2 (*continued*)

Sample		Cd ppb	Cd ng	% of total Cd eluted	Yield (%)	Blank (%)	$^{118}Sn/^{111}Cd$	$^{115}In/^{111}Cd$	$^{105}Pd/^{111}Cd$	N	$\varepsilon^{106}Cd$	$\varepsilon^{108}Cd$	$\varepsilon^{110}Cd$	$\varepsilon^{112}Cd$	$\varepsilon^{113}Cd$	$\varepsilon^{114}Cd$
Allende PB Mean	CV3	200								3	-0.03 ± 2.07	-0.59 ± 2.24	$-0.17 \pm 0.36^{\dagger}$	$-0.10 \pm 0.23^{\dagger}$	$-0.36 \pm 0.27^{\dagger}$	$-0.03 \pm 0.24^{\dagger}$
MIL 090001	CR2	200	107		83	0.03	3.7E−04	3.6E−06	2.3E−05	1	0.79 ± 0.78	0.51 ± 0.93	0.12 ± 0.16	-0.01 ± 0.13	-0.30 ± 0.18	-0.07 ± 0.15
EET 92048	CR2	200					1.8E−04	7.5E−06	2.7E−05	1	0.68 ± 0.91	0.74 ± 1.14	0.18 ± 0.24	0.04 ± 0.19	-0.15 ± 0.22	0.07 ± 0.18
	CR2	200					2.2E−04	2.2E−06	2.6E−05	1	0.28 ± 0.78	0.25 ± 0.93	0.08 ± 0.16	-0.01 ± 0.13	-0.16 ± 0.18	-0.08 ± 0.15
EET 92048 Mean	CR2	200	230		96	0.02				2	$0.48 \pm 1.25^{\dagger}$	$0.50 \pm 1.08^{\dagger}$	$0.13 \pm 0.36^{\dagger}$	$0.01 \pm 0.23^{\dagger}$	$-0.16 \pm 0.27^{\dagger}$	$0.00 \pm 0.24^{\dagger}$
GRA 06100	CR2	1	0.7			4.33	7.2E−02	1.6E−03	5.8E−03	1	192 ± 162	160 ± 220	-2.81 ± 9.19	-8.33 ± 6.96	-9.89 ± 7.55	-10.5 ± 8.4
Indarch	EH4	200					2.7E−04	1.1E−05	2.9E−05	1	0.31 ± 0.74	0.94 ± 1.00	0.18 ± 0.28	0.01 ± 0.20	-0.44 ± 0.26	0.23 ± 0.24
	EH4	200					1.8E−04	6.9E−06	2.3E−05	1	0.30 ± 0.75	0.02 ± 1.23	0.14 ± 0.28	0.02 ± 0.15	-0.47 ± 0.18	0.24 ± 0.15
	EH4	200					2.2E−04	8.9E−06	2.6E−05	1	-0.50 ± 0.94	-0.62 ± 1.37	0.14 ± 0.27	0.13 ± 0.13	-0.58 ± 0.18	0.11 ± 0.17
	EH4	200					1.4E−04	1.2E−05	3.1E−05	1	-0.47 ± 0.96	-0.47 ± 1.19	0.18 ± 0.31	0.11 ± 0.14	-0.37 ± 0.21	0.19 ± 0.16
	EH4	200					1.5E−04	4.7E−06	2.8E−05	1	-0.05 ± 0.78	-0.84 ± 0.93	0.19 ± 0.16	0.18 ± 0.13	-0.44 ± 0.18	0.21 ± 0.15
Indarch Mean	EH4	200	482		85	0.01				5	$-0.08 \pm 1.25^{\dagger}$	-0.19 ± 1.42	$0.17 \pm 0.36^{\dagger}$	$0.09 \pm 0.23^{\dagger}$	$-0.46 \pm 0.27^{\dagger}$	$0.20 \pm 0.24^{\dagger}$
Jbilet Winselwan Leach fractions																
1b − 50% HAc		200	126	25	76	0.07	3.3E−04	1.9E−05	2.3E−05	1	0.06 ± 0.96	0.02 ± 1.19	-0.06 ± 0.31	-0.06 ± 0.14	-0.66 ± 0.21	0.14 ± 0.16
2a − 1 M HNO_3		200					1.9E−04	4.3E−06	2.1E−05	1	-0.41 ± 0.91	-0.55 ± 1.14	-0.08 ± 0.24	-0.10 ± 0.19	-0.59 ± 0.22	0.16 ± 0.18
		200					2.1E−04	−2.4E−06	2.4E−05	1	0.59 ± 0.96	0.28 ± 1.19	-0.24 ± 0.31	-0.11 ± 0.14	-0.72 ± 0.21	0.05 ± 0.16
2a Mean		200	235	46	85	0.04				2	0.09 ± 1.42	-0.13 ± 1.17	$-0.16 \pm 0.36^{\dagger}$	$-0.10 \pm 0.23^{\dagger}$	$-0.66 \pm 0.27^{\dagger}$	$0.11 \pm 0.24^{\dagger}$
2b − 4 M HNO_3		200	129	25	97	0.03	2.8E−04	1.2E−05	2.8E−05	1	-1.30 ± 0.96	-1.33 ± 1.19	-0.11 ± 0.31	-0.16 ± 0.14	-0.79 ± 0.21	0.06 ± 0.16
3a − 6 M HCl, RT		3.4					6.0E−03	1.6E−04	1.3E−03	1	-11.7 ± 32.1	-47.5 ± 40.1	-0.01 ± 3.56	2.83 ± 2.42	-0.86 ± 2.78	2.28 ± 2.93
		3.4					7.5E−03	1.7E−04	1.3E−03	1	15.1 ± 29.6	-10.2 ± 35.0	0.44 ± 2.56	1.45 ± 1.38	1.40 ± 3.11	1.59 ± 1.94
		3.4					7.7E−03	1.4E−04	1.3E−03	1	13.4 ± 29.6	16.8 ± 35.0	3.28 ± 2.56	1.25 ± 1.38	-0.92 ± 3.11	0.14 ± 1.94
3a Mean		3.4	16.7	3.3	104	0.11				3	$5.6 \pm 37.8^{\dagger}$	-13.6 ± 64.7	$1.24 \pm 3.65^{\dagger}$	$1.84 \pm 2.32^{\dagger}$	-0.13 ± 2.65	1.34 ± 2.18
3b + c − 6 M HCl, 80 °C		3.4	2.0	0.4	87	0.93	2.3E−02	6.3E−04	1.6E−03	1	4.4 ± 47.1	-36.3 ± 65.1	-0.80 ± 4.48	1.33 ± 2.88	-1.12 ± 1.95	1.20 ± 3.15
4 – 13.5 M HF + 3 M HCl		2.3	1.5	0.3	86	1.44	4.9E−02	1.6E−03	3.1E−03	1	-65.1 ± 61.4	-157 ± 60	0.02 ± 3.84	3.32 ± 5.19	-0.45 ± 7.25	0.44 ± 5.88
5 − conc. HF + HNO_3, PB		2.3	1.5	0.3	43	3.34	4.9E−02	9.5E−04	2.4E−03	1	0.6 ± 63.0	0.1 ± 55.6	0.64 ± 7.59	-0.02 ± 3.70	-4.82 ± 6.26	-1.22 ± 2.93
Jbilet Winselwan Leachates Total			511													

All Cd isotope data are internally normalised relative to $^{116}Cd/^{111}Cd$. For individual measurements, the 2SD drift corrected reproducibility of the Alfa Aesar Cd standard on the measurement day is given. For averages of the bulk meteorites and leachates, the 2SD of their repeat analyses are shown or the 2SD of Nod-P-1 measured at the same concentration (marked with †), whichever is larger. This approach was used due to the low number of repeats possible for some of the meteorites. The column "Cd ppb" denotes the sample concentration of the analysis, whereas the column "Cd ng" refers to the total amount of Cd recovered after the full separation procedure. For leachates, this is also given as the percentage of the total Cd collected from all the leach fractions. The yield of GRA 06100 is not reported here due to large uncertainties caused by the low Cd content of this sample. RT: room temperature; HP: hotplate digestion; PB: Parr® bomb digestion; N: number of individual measurements.

* Number of measurement sessions are given instead of individual measurements.

Data from Friebel et al. (2020).

cult to understand (Gault-Ringold and Stirling, 2012). A later study proposed that the analytical artifacts induced by TRU resin organics are due to resultant changes in the plasma conditions and thereby instrumental mass bias (Murphy et al., 2016). Our study also utilizes TRU resin for the second separation step (Friebel et al., 2020). Samples are, however, further purified in a third and fourth separation step using the AG 1-X8 anion-exchange resin. While calibrating the third column, we determined that the majority (~80–90%) of the total P eluted with the matrix fraction. This, together with the use of the Eichrom Pre-filter resin during the second column chemistry, helps to avoid P and organics eluted from the TRU resin in the final Cd fraction (Friebel et al., 2020).

Another element that can potentially interfere with Cd isotopes is K ($^{39}K + {}^{40}Ar + {}^{16}O + {}^{16}O \rightarrow {}^{111}Cd$). Due to their high backgrounds, K and P content of the samples are difficult to determine from mass-scans on the Nu Plasma II. Therefore, an aliquot of the final Cd fractions from four samples with sufficient Cd contents (Lake Zürich I, Jbilet Winselwan, Indarch and Murchison) were analysed on an Element XR ICP-MS. Their concentrations ranged from 3–21 ppb for P and 0.1–4.7 ppb for K, yielding K/Cd ratios between 6.41×10^{-4} and 1.34×10^{-2}, and P/Cd ratios between 1.18×10^{-2} and 4.14×10^{-2}. These values were taken as estimates for doping tests to assess the effects of these elements on Cd isotopes.

For testing P, the 200 ppb Cd Alfa Aesar standard solution was doped with 5 ppb, 10 ppb, 40 ppb and 80 ppb P (P/Cd ratios of 2.5×10^{-2} to 4.0×10^{-1}). No effects are observed for additions of 5 and 10 ppb P. However, at 40 and 80 ppb P, the data show resolvable negative offsets on ε^{110}Cd and ε^{112}Cd, hints on ε^{114}Cd, ε^{106}Cd and ε^{108}Cd, and a potential positive effect on ε^{113}Cd (Fig. S1). The results can be explained by an interference on ^{111}Cd from a potential P argide interference, but the ε^{113}Cd data requires either (i) another interference, or more likely (ii) an analytical artifact or matrix effect that influences ^{113}Cd only. Overall, the P doping tests indicate that the tolerance limit is between 5×10^{-2} and 2×10^{-1} P/Cd. This is above the purified sample solution contents determined and, hence, P is not expected to affect the accuracy of the obtained Cd isotope data.

Doping tests of K were performed using 0.05 ppb to 30 ppb K, which correspond to K/Cd ratios of 2.5×10^{-4} to 1.5×10^{-1}. The data show no systematic offsets with increasing K concentration (Fig. S1). Therefore, K interferences in this range are negligible. However, the data display

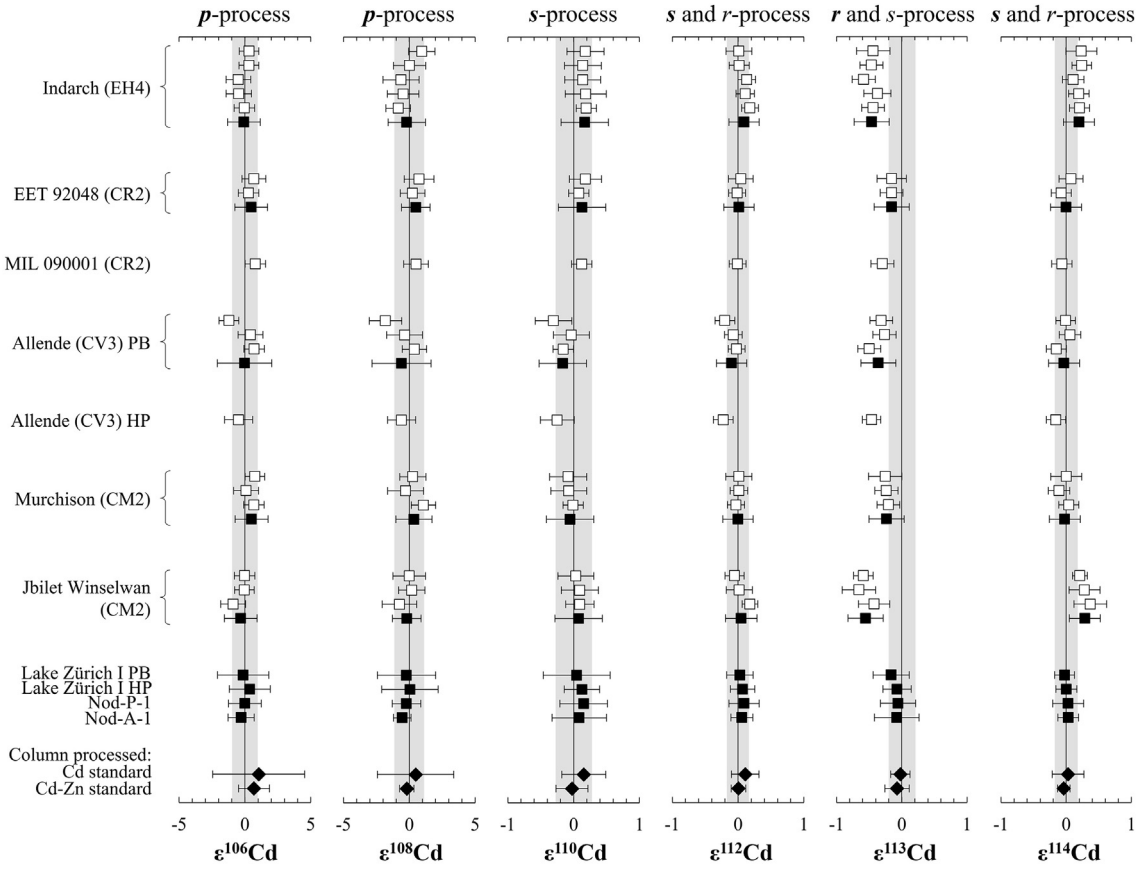

Fig. 1. Cadmium isotope data for high-precision (200 ppb Cd) bulk sample measurements, internally normalised to $^{116}Cd/^{111}Cd$. Single measurements are shown with open symbols and averages with filled symbols. Error bars are the same as in Table 2. For each Cd isotope, the dominant nucleosynthetic process is shown in bold above the graphs. The grey band indicates the average drift corrected daily reproducibility (2SD) of the 200 ppb Cd Alfa Aesar standard solution.

some scatter at several different concentrations that vary from one measurement session to another (Fig. S1). This indicates that K addition to the Alfa Aesar Cd standard solution can induce small matrix effects. To assess potential shifts in the Cd isotope data originating from K in the sample solution, doping tests were regularly performed before sample analysis to monitor data quality. Additionally, column processed standards and/or terrestrial samples were always measured as a first test before the meteorite samples. Meteorites were only analysed when the doping tests and the terrestrial samples both gave accurate and precise results.

2.6. Yields and procedural blanks

The overall yields after the digestion and separation procedure were on average 70% or higher. For some of the low concentration samples, in particular GRA 06100, yields are more variable, due to difficulties in estimating their initial Cd content from a small aliquot (~1%) (Friebel et al., 2020) (Table 2). Blanks from the Parr® bomb digestion ranged from ~2 to 28 pg Cd per vial, and were between ~4 and 141 pg Cd in total per sample. The blanks of the complete separation procedure were ≤100 pg Cd. The total procedural blank contribution for samples and leach fractions ranged from ~0.01% to 4.33% (Table 2). These levels are insignificant, in particular considering the large analytical uncertainties on the low concentration sample measurements, and therefore no blank correction was applied.

3. RESULTS

Cadmium isotope data of standards and terrestrial samples, as well as bulk chondrites and acid leachates of Jbilet Winselwan, are presented in Table 2. Terrestrial samples and column processed standards at all measured concentrations (200, 3.4, 2.3 and 1 ppb Cd) overlap with the bracketing Alfa Aesar Cd standard considering their analytical uncertainties.

The averages of the bulk chondrites measured at high-precision (200 ppb Cd) display identical Cd isotope compositions to the terrestrial samples and standard for ε^{106}Cd, ε^{108}Cd, ε^{110}Cd and ε^{112}Cd within uncertainties (Table 2, Fig. 1). We consider an offset as resolvable in the sample data if the data do not overlap with 0 within the reported analytical uncertainties. The ε^{113}Cd data show resolved negative values for all bulk chondrites, apart from EET 92048 and Murchison, which also trend towards negative values (Fig. 1). Hints of potential positive ε^{114}Cd values are observed for Jbilet Winselwan and Indarch.

The first three Cd-rich leach fractions of Jbilet Winselwan measured at high-precision agree within uncertainties with the bulk rock results, with resolvable negative ε^{113}Cd values of a similar magnitude and no ε^{114}Cd offsets from the bracketing Cd standard solution (Table 2, Fig. 2). The last four Cd-poor leachates measured at lower concentrations (3.4 and 2.3 ppb Cd) display identical Cd isotope compositions to the terrestrial Alfa Aesar standard, with the exception of negative ε^{106}Cd and ε^{108}Cd values for leach 4 (HF + HCl step) (Fig. 2).

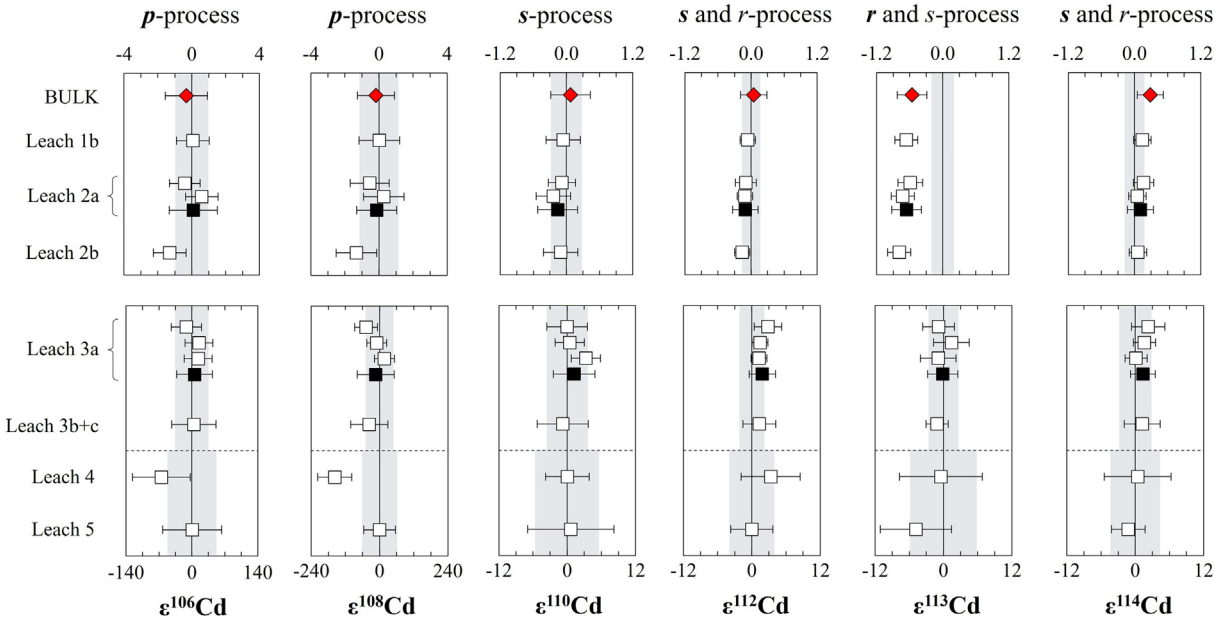

Fig. 2. Cadmium isotope compositions of bulk and leach fractions from Jbilet Winselwan, internally normalised to ^{116}Cd/^{111}Cd. Single measurements are shown with open and averages with filled symbols. Note the different scales used for the top (high-precision) and the bottom (low-precision) data. The dominant nucleosynthetic production is indicated in bold for each Cd isotope. Error bars are the same as in Table 2. The grey bands represent the average drift corrected daily reproducibility (2SD) of the Alfa Aesar Cd standard solution measured at the same concentration as the samples, as given in Table 2 (200 ppb Cd – Bulk, Leach 1b, 2a and 2b; 3.4 ppb Cd – Leach 3a and 3b + c; 2.3 ppb Cd – Leach 4 and 5).

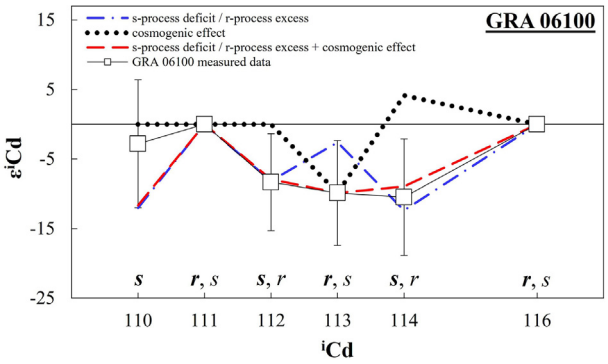

Fig. 3. Cadmium isotope data of GRA 06100 shown for the more abundant isotopes ^{110}Cd to ^{116}Cd, internally normalised to ^{116}Cd/^{111}Cd. Error bars represent the 2SD drift corrected reproducibility of the Alfa Aesar Cd standard on the day of the measurement. The dominant nucleosynthetic production process is shown in bold. Also depicted are modelled results for a pure nucleosynthetic and cosmogenic effect, and a combination of the two for comparison. Cosmogenic effects were modelled by assuming a deficit on ^{113}Cd and a corresponding increase in ^{114}Cd that scale with their natural abundance. For the nucleosynthetic model, a deficit or excess was assumed on ^{111}Cd. This was scaled with the relative contribution of each Cd isotope from the *s*- and *r*-process and its magnitude was varied until the offsets best matched our sample data (*s*- and *r*-process abundances from Bisterzo et al. (2011) and references therein). The *s*-process deficit generates the same pattern as an *r*-process excess for the more abundant Cd isotopes (see e.g. Fig. 4), therefore they are shown as one line. The *p*-process isotopes ^{106}Cd and ^{108}Cd are not shown because the expected effects are more than a factor of 10 smaller than the measurement precision on these low abundance isotopes.

The bulk chondrite GRA 06100 could only be measured at 1 ppb Cd. It shows resolvable negative shifts for ε^{112}Cd, ε^{113}Cd and ε^{114}Cd (Fig. 3), and trends towards positive ε^{106}Cd and ε^{108}Cd values with a resolved ε^{106}Cd offset of $+192 \pm 162$ (Table 2).

4. DISCUSSION

4.1. Column processed terrestrial standards and samples: accuracy and precision

To assess the accuracy and precision of our data an aliquot of Nod-A-1 and three separately digested aliquots of Nod-P-1 were processed through the separation procedure in ~0.1 g fractions containing ~600–2000 ng Cd. Repeated measurements of Nod-P-1 at 200 ppb Cd (2SD, n = 25) yield values identical to the Alfa Aesar Cd standard solution within analytical uncertainties with 0.00 ± 1.25 for ε^{106}Cd, -0.22 ± 1.08 for ε^{108}Cd, 0.15 ± 0.36 for ε^{110}Cd, 0.09 ± 0.23 for ε^{112}Cd, -0.06 ± 0.27 for ε^{113}Cd and 0.03 ± 0.24 for ε^{114}Cd (Table 2). The 200 ppb data of Nod-A-1 and Lake Zürich I are very similar (Table 2). The accuracy of the analytical procedure was also established as described in Friebel et al. (2020). It included three column processed ~500 ng aliquots of the Alfa Aesar Cd standard solution, four mixed ~200 ng Cd and ~80 µg Zn standard aliquots and eight aliquots of the lake Zürich sediment processed in ~200–500 ng Cd fractions. These are very similar to the amount of Cd in the bulk meteorite samples (~100–500 ng Cd). Despite the different sample matrices, the data displayed very similar accuracy and reproducibility to Nod-P-1, supporting the robustness of our method. Here, we extended the tests to lower concentration analyses (3.4, 2.3 and 1 ppb Cd; Table 2). With lower Cd concentrations the precision decreases, as expected from reduced counting statistics and lower signal-to-noise ratio. However, in general accurate data is obtained that overlaps with the bracketing Alfa Aesar Cd standard within analytical uncertainties.

4.2. Nucleosynthetic homogeneity of Cd isotopes in the early solar system

The bulk rock samples of carbonaceous and enstatite chondrites, with the exception of GRA 06100, were all measured at 200 ppb Cd to obtain high precision Cd isotope data. The most pronounced isotopic variations are present for Jbilet Winselwan with an ε^{113}Cd of -0.56 ± 0.27 and Indarch with -0.46 ± 0.27 (Table 2). A very small positive ε^{114}Cd offset is only just resolvable for Jbilet Winselwan at $\varepsilon^{114}\text{Cd} = +0.29 \pm 0.24$. This indicates a potential inverse correlation between the ^{113}Cd and ^{114}Cd data (Fig. 1).

To explain the negative ε^{113}Cd values with the preservation of presolar grains from a specific nucleosynthetic source, an *s*-process deficit or *r*-process excess would be required (Fig. 4). To generate an ε^{113}Cd offset of −0.56, as observed for Jbilet Winselwan (and very similar for Indarch), an *s*-process deficit/*r*-process excess would produce concomitant negative effects of −1.72 or larger for ε^{110}Cd, ε^{112}Cd and ε^{114}Cd (Fig. 4). This is not observed (Fig. 1). The expected negative shift in ε^{114}Cd is also in conflict with the slightly positive ε^{114}Cd identified for Jbilet Winselwan. Moreover, large concomitant positive (>2 ε) or negative offsets (≤−2 ε) would be expected for both

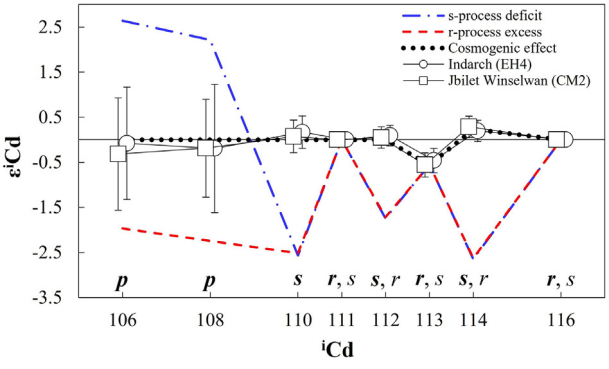

Fig. 4. Cadmium isotope data of Jbilet Winselwan (CM2) and Indarch (EH4) shown against the modelled offsets for thermal neutron capture effects and an *s*-process deficit/*r*-process excess. Data are internally normalised to ^{116}Cd/^{111}Cd. For easier comparison, the models were scaled to match the ε^{113}Cd values measured for Jbilet Winselwan and Indarch. For each Cd isotope, the dominant nucleosynthetic process is indicated in bold. Cosmogenic and nucleosynthetic effects were modelled using the same approach as for Fig. 3.

ε^{106}Cd and ε^{108}Cd with an *s*-process deficit or *r*-process excess, respectively. Variations of this magnitude are easily resolved with our analytical precision, but were not present. From this, it is evident that the offsets of our analysed bulk samples are not related to nucleosynthetic Cd isotope variations.

Similarly, the first three leachates of Jbilet Winselwan are in good agreement with the bulk rock results and therefore, they cannot be reproduced with an *s*-process deficit or *r*-process excess model either. Of the later Cd-poor leachates, only leach 4 (HF + HCl step) displays resolvable Cd isotope variations relative to the terrestrial Alfa Aesar standard in the form of negative ε^{106}Cd and ε^{108}Cd values (Fig. 2). These most likely originate from traces of Cu in the purified sample solution identified in the mass scans prior to isotope analysis. Copper creates an interference on mass 105 ($^{65}Cu^{40}Ar$) used for the Pd correction, which results in an overcorrection on ^{106}Cd and ^{108}Cd and thus in negative offsets in these isotopes.

Differences between hotplate and bomb digested samples were previously reported for other elements, e.g., Zr, relating to the incomplete dissolution of refractory phases such as presolar silicon carbide (SiC) grains (Akram et al., 2013). Our results show that the hotplate and bomb digested Allende samples have identical Cd isotope compositions within analytical uncertainties (Table 2, Fig. 1). This provides further evidence in addition to the leach-experiment data that no significant amount of Cd with an anomalous isotope signature is hosted in the more acid-resistant fractions of Jbilet Winselwan and Allende.

Overall, our Cd isotope data provide compelling evidence that no resolvable nucleosynthetic Cd isotope variations are present in bulk carbonaceous chondrites or their components. However, we cannot exclude the presence of heterogeneities below our detection limit. Our data imply that Cd was efficiently homogenised after nucleosynthesis either in the interstellar medium or during solar system formation and that known predominantly refractory presolar phases (e.g. nanodiamonds, SiC grains, presolar silicates and oxides) contain very minor amounts of anomalous Cd, not able to cause isotopic variations outside our analytical precision.

4.3. Implications of nucleosynthetic homogeneity in moderately volatile elements

In agreement with our Cd data, other moderately volatile and chalcophile elements, such as Te (Fehr et al., 2005) and Se (Labidi et al., 2018), also lack resolvable nucleosynthetic variability at the bulk meteorite scale. Our companion Sn isotope study on the same samples as presented here shows very limited nucleosynthetic variability (Friebel, 2018; Friebel et al., 2020). In addition, the moderately volatile elements Ag and Tl provide no evidence for nucleosynthetic heterogeneity, although these data are more difficult to assess because both elements have only two isotopes and different processes (e.g. radioactive decay of the short-lived nuclides ^{107}Pd and ^{205}Pb or mass-dependent isotope fractionation) are not easily distinguished from each other (Schönbächler et al., 2008; Baker et al., 2010). Because Cd does not display nucleosynthetic isotope variations, this is also expected for other moderately volatile elements, including Ag and Tl, aiding their robustness as early solar system chronometers.

The absent or limited nucleosynthetic variability in moderately volatile elements stands in strong contrast with that of refractory elements in the same mass range such as Zr, Mo, Ru and Pd that show a depletion of *s*-process material in carbonaceous chondrites relative to Earth (e.g. Dauphas et al., 2004; Chen et al., 2010; Burkhardt et al., 2011; Akram et al., 2015; Fischer-Gödde et al., 2015; Poole et al., 2017; Ek et al., 2020). Ek et al. (2020) showed that Pd exhibits *s*-process variations of a smaller magnitude than expected, due to its lower 50% T_C leading to incomplete condensation around AGB stars. In the framework of this model, no measurable variations in Cd isotopes are predicted, because Cd is significantly more volatile than Pd. Hence, the absent or limited nucleosynthetic variability in Cd and other moderately volatile elements supports that these elements did not readily condense into refractory presolar grains around AGB stars, but preferentially stayed in the gas phase (e.g. Lodders and Fegley, 1997). Isotopes in the gas phase were then homogenised in the interstellar medium and the original nucleosynthetic signature was diluted down to average local interstellar medium composition. Furthermore, Ek et al. (2020) discusses that if moderately volatile elements condensed around AGB stars, they were most likely incorporated into fragile phases, which were then readily destroyed and homogenised in the interstellar medium. Subsequently, these elements with average local interstellar medium composition were incorporated into interstellar dust, which contributed to the molecular cloud from which our solar system formed. Our new Cd isotope data is thus in very good agreement with the model proposed by Ek et al. (2020). The data also allow for the possibility that further mixing of Cd isotopes occurred during solar system formation such as during (i) thermal processing in the protoplanetary disk (e.g. calcium-aluminium-rich inclusion (CAI) and chondrule formation) or (ii) aqueous alteration on the carbonaceous chondrite parent bodies.

4.4. Potential carrier phases of Cd in carbonaceous chondrites

Our leaching experiment reveals Cd isotope homogeneity in the different leach fractions of the CM2 chondrite Jbilet Winselwan (Table 2, Fig. 2). This is in general agreement with results from the moderately volatile element Te. Leachates of Orgueil, Allende and Murchison display Te isotopic homogeneity (Fehr et al., 2006). However, there are hints of positive ε^{128}Te and ε^{130}Te values in the 4 M HNO_3 fraction (leach 2) of Murchison and the final Parr® bomb fraction (leach 5b) of Allende, indicating a potential component in these meteorites with an *s*-process deficit (or *r*-process excess). In contrast, another study suggested an *r*-process deficit component for Te in the final acid-resistant residue of Allende (Fukami and Yokoyama, 2017). It was proposed that this might reflect a depletion in nanodiamonds that carry an *r*-process excess (Richter et al., 1998;

Maas et al., 2001) or glassy carbon as presolar carriers of Te hosting such a component (Fukami and Yokoyama, 2017). The differences between the results of Fehr et al. (2006) and Fukami and Yokoyama (2017) might then reflect different degrees of leaching of these carrier phases by the employed digestion procedures. Additionally, the Sn isotope data of our leachate 5 (conc. HF + HNO_3) suggests the presence of an acid-resistant presolar phase (e.g. SiC grains or presolar oxides) with an *s*-process excess (or *r*-process deficit) in Jbilet Winselwan (Friebel, 2018). This result indicates that moderately volatile elements (e.g. Sn) can be present in refractory presolar grains that preserve their original nucleosynthetic isotope composition. This stands in contrast with the observed Cd isotopic homogeneity, indicating that Cd was originally not present in the preserved Sn carrier phase. Overall, the differences observed between Sn, Cd and Te, despite their similar volatility, most likely stem from their different carrier phases. The slightly more volatile and chalcophile Cd must have been incorporated into presolar carriers to a lesser extent than Sn, and potentially also Te, perhaps into phases more susceptible to (i) recycling in the interstellar medium or (ii) thermal and aqueous alteration on the meteorite parent body than nanodiamonds and SiC grains. This provides further evidence that the condensation behaviour of elements in stellar environments is critical for the preservation of nucleosynthetic anomalies and that the isotopic homogeneity of Cd and other moderately volatile elements is mainly set by the lack of condensation into refractory presolar grains around stars.

The Cd distribution in the leach fractions of Jbilet Winselwan can provide further insight about the potential mineral phases hosting Cd in carbonaceous chondrites. Jbilet Winselwan is described as a brecciated chondrite that experienced variable amounts of aqueous alteration and thermal metamorphism, containing heterogeneously distributed carbonates (King et al., 2019). Our leaching experiment shows that the first step using 50% HAc (leach 1b) released a significant amount (25%) of the total Cd in Jbilet Winselwan (Table 2). This acid step targets the most easily dissolved phases, including carbonates, sulphates and sulphides (Rotaru et al., 1992). After the next two leach steps using 1 M HNO_3 (leach 2a, 46%) and 4 M HNO_3 (leach 2b, 25%), almost all of the total Cd (~96%) was released (Table 2). These two steps most likely reflect the further dissolution of sulphides because Jbilet Winselwan has a low Fe-Ni metal content (<1 vol.%) (King et al., 2019). Since Cd is a chalcophile element, it is expected to predominantly occur in sulphur-bearing minerals, such as troilite, which agrees with our observations.

The next two 6 M HCl leach steps (leach 3a and 3b + c) together yield <4% of the total Cd (Table 2). The HF treated leach fractions (leach 4 and 5) contain even less Cd (<1% of the total) (Table 2). These imply that the silicates and the more acid-resistant refractory phases, such as presolar SiC grains, host minute amounts of Cd. Therefore, our leach experiment of Jbilet Winselwan demonstrates that only a very minor fraction of the total Cd budget in carbonaceous chondrites is hosted in high-temperature components (e.g. presolar phases, CAIs and chondrules). This is best explained by Cd loss to the vapour phase during heating events due to its relatively high volatility. While a majority of the Cd budget was likely already homogenised in the interstellar medium, the scarcity of Cd in high temperature phases formed in the solar system indicates that further Cd evaporation/condensation and homogenisation has taken place in the solar nebula.

Moreover, since most Cd was released in the first leaching steps, which mainly dissolve phases formed during aqueous alteration, additional mobilisation and homogenisation likely occurred on the parent body during aqueous alteration and potentially during thermal metamorphism. This is also supported by previous studies (Wombacher et al., 2003; Wombacher et al., 2008), who concluded based on the combined Cd and Zn concentration and isotopic record that Cd isotopes strongly fractionate during heating of a parent body. They also report evidence of Cd loss during chondrule formation followed by partial recondensation of Cd into chondrules during cooling. In summary, mixing of Cd isotopes likely occurred in the interstellar medium, but also during thermal processing in the protoplanetary disk (e.g. CAI and chondrule formation) and aqueous alteration on the carbonaceous chondrite parent bodies.

4.5. Sources of Cd isotope variations in GRA 06100

The CR2 chondrite GRA 06100 was particularly challenging to measure because it is depleted in Cd (~1 ppb) compared to the other two analysed CR2 chondrites (~100–200 ppb Cd) (Table 2). The measurement was performed at 1 ppb Cd and therefore uncertainties are considerably larger (several ε) for this sample compared to the high-precision Cd isotope data obtained for all other bulk samples. GRA 06100 shows resolvable negative offsets for ε^{112}Cd, ε^{113}Cd and ε^{114}Cd (Fig. 3), and a positive ε^{106}Cd offset (Table 2). For the more abundant Cd isotopes, internal normalisation of the data using ^{113}Cd/^{111}Cd provides a resolvable positive offset in ^{116}Cd (Fig. S2a). Normalisation using ^{112}Cd/^{114}Cd and ^{110}Cd/^{114}Cd reveal no variations (Fig. S2b and c). For the two low abundance Cd isotopes, using all three normalising ratios give the same positive trends with a resolved ε^{106}Cd from the bracketing standard.

The Cd isotope data for GRA 06100 reveal a different isotope pattern compared to the other bulk chondrites. Matrix effects and interferences can increase at such low Cd concentration and therefore, were carefully investigated. However, doping tests with Zr, Zn, K, P, Pd and Sn at similar levels to what was estimated for the purified GRA 06100 sample solution resulted in no offsets that could explain its Cd isotope composition (Table S2).

Therefore, to evaluate the origin of the negative ε^{112}Cd, ε^{113}Cd and ε^{114}Cd values, we modelled the expected Cd isotope shifts for (i) an *s*-process deficit/*r*-process excess, (ii) cosmogenic effects and (iii) a combination of the two (Fig. 3). Pure neutron capture induced effects due to exposure to galactic cosmic rays cannot explain the GRA 06100 data, because they affect ^{113}Cd and ^{114}Cd only. An *s*-process deficit or *r*-process excess could replicate the GRA 06100 Cd isotope data considering the analytical

uncertainties, however, the combined nucleosynthetic and cosmogenic pattern provides the best match (Fig. 3). This is also supported when using the three other Cd ratios for internal normalisation (Fig. S2). The exposure age of GRA 06100 is unknown, however, CR chondrites have an average CRE age of ~8 Ma with a range from 1 to 25 Ma (Herzog and Caffee, 2014). The combined nucleosynthetic and cosmogenic model that fits the measured data (internally normalised to $^{116}Cd/^{111}Cd$) requires a large cosmogenic contribution that shifts the $\varepsilon^{113}Cd$ value by −7. Such effects would be realistic according to the GCR model (Leya and Masarik, 2013) if the exposure age of GRA 06100 is close to ~10 Ma or longer, slightly above the current CR average.

GRA 06100 shows a large positive $\varepsilon^{106}Cd$ offset (Table 2), while $\varepsilon^{108}Cd$ is also positive, but not resolved from the terrestrial standard. This fits with an *s*-process deficit (Fig. 3), but the measured values are too extreme. An *s*-process deficit that matches the other Cd isotope data produces predicted collateral effects of ~10–12 ε for ^{106}Cd and ^{108}Cd, which are not resolvable at the current analytical precision. Therefore, an additional nucleosynthetic excess in *p*-process isotopes would be required, if the positive $\varepsilon^{106}Cd$ represents a true nucleosynthetic isotope anomaly and not an analytical artifact. Refractory elements such as Mo, Sm and Nd display variations in *p*-process isotopes in bulk carbonaceous chondrites. However, these have been attributed to variable amounts of *s*-process materials in these meteorites (Burkhardt et al., 2011; Bouvier and Boyet, 2016). Other *p*-process isotopes such as ^{190}Pt are homogenously distributed in the solar system (Hunt et al., 2017). This hints at the possibility that the positive $\varepsilon^{106}Cd$ value might be caused by an analytical problem.

The low Cd content of GRA 06100 compared to the other two investigated CR2 chondrites (EET 92048 and MIL 090001) suggests that it experienced major volatile loss. However, this sample has a normal Zn content (Mahan et al., 2018). Previous work on GRA 06100 reported evidence for aqueous alteration and open-system thermal metamorphism, most likely as a result of impact processing (e.g. Abreu and Bullock, 2013; Briani et al., 2013). Aqueous alteration can result in element mobilisation, such as for Zn (Friedrich et al., 2018). Additionally, shock metamorphism can also generate mobilisation, volatilisation and re-condensation of volatile and moderately volatile elements (e.g. Wombacher et al., 2008; Mahan et al., 2018). To account for the Cd poor nature of GRA 06100 compared to its Zn content, it is plausible that the slightly more volatile nature of Cd played a role. This is also reflected by ordinary chondrites and some enstatite and carbonaceous chondrite groups that experienced thermal metamorphism. They show large variations in their Cd concentrations relative to Zn (Wombacher et al., 2008).

Estimates for mass-dependent Cd isotope fractionation based on our data indicate that the sample is strongly enriched in heavy Cd isotopes (up to +1.2–1.8 ‰ per amu based on the data for $^{113}Cd/^{111}Cd$, $^{116}Cd/^{111}Cd$, $^{112}Cd/^{114}Cd$ and $^{110}Cd/^{114}Cd$). It is conceivable that Cd evaporated (i) during the impact as a molecule e.g., CdS or (ii) its evaporation in monoatomic form did not follow the exponential (kinetic) mass fractionation law that was applied to the data to correct for natural and instrumental Cd isotope fractionation. Experiments indicate that Cd evaporation into a vacuum does not entirely follow the kinetic/exponential law (Wombacher et al., 2004). Both cases (i) and (ii) can lead to apparent mass-independent Cd isotope variations when compared to the bracketing standard (e.g. see Wombacher et al., 2004). Theoretically, the observed pattern of GRA 06100 can be generated by option (i) molecular evaporation or (ii) different fractionation law e.g., using the power or equilibrium fractionation law. The problem with this interpretation is that the observed mass-dependent shift (+1.2–1.8 ‰ per amu) and the relatively normal fractionation factor observed during MC-ICPMS analysis (−2.1 for $^{116}Cd/^{111}Cd$, compared to −1.9 for the measured standards) do not allow for the large negative shifts of several epsilon for e.g. $\varepsilon^{112,113,114}Cd$ required by the GRA 06100 data.

In summary, it is not clear what caused the Cd isotope composition of GRA 06100. It could be analytical, generated by a combined nucleosynthetic and cosmogenic signal or the leftover of inadequate mass bias correction. It is evident that this sample is unique in the current data set and a firmer answer will require further investigation.

4.6. Thermal neutron capture effects on Cd isotopes

The negative $\varepsilon^{113}Cd$ offsets observed for the majority of the bulk samples are best explained as the effect of irradiation with GCR (Fig. 4). This reaction (^{113}Cd (n,γ) ^{114}Cd) results in $\varepsilon^{114}Cd/\varepsilon^{113}Cd$ ratios of −0.42, which is set by the natural abundance of ^{113}Cd (12.22%) and ^{114}Cd (28.73%). The collateral $\varepsilon^{114}Cd$ effect will not be resolvable within the current analytical precision (±0.24 based on analyses of Nod-P-1, 2SD, n = 25), if the $\varepsilon^{113}Cd$ value is between 0 and −0.57. Therefore, it is possible to observe offsets in $\varepsilon^{113}Cd$ without resolvable effects in $\varepsilon^{114}Cd$. As a first test, the effects of neutron capture on Cd isotopes were modelled by assuming that the neutron capture on ^{113}Cd is the only relevant reaction. To match the largest $\varepsilon^{113}Cd$ offset observed for Jbilet Winselwan at −0.56, our model predicts an $\varepsilon^{114}Cd$ value of +0.23. This fits the $\varepsilon^{114}Cd$ value of Jbilet Winselwan of $+0.29 \pm 0.24$ very well (Fig. 4). The model results also agree with the Indarch data (Fig. 4). From this it follows that all the other investigated samples that show smaller $\varepsilon^{113}Cd$ values are not expected to display resolvable $\varepsilon^{114}Cd$ excesses, which is in agreement with our data (Table 2).

Neutron capture effects in meteorites depend on several factors including the chemical composition of the meteorite, radius, shielding depth and cosmic-ray exposure (CRE) age (Leya and Masarik, 2013). All our samples are chondrites. As such, their similar bulk chemical composition should not generate large differences in neutron capture efficiencies. However, the higher water content of carbonaceous chondrites might enhance the magnitude of thermal neutron capture effects (Leya and Masarik, 2013). The radius of the meteoroid and the depth of the analysed samples are often unknown, but their CRE ages can serve

as a good first indication for the magnitude of expected neutron capture effects. Indarch has the longest CRE age of 12.1 ± 2.5 Ma (Eugster et al., 2007), followed by Allende at 4.8 ± 0.5 Ma and Murchison at 1.6 ± 0.3 Ma (Roth et al., 2011). These ages represent upper estimates. Published ages for EET 92048 and MIL 090001 are not available, but CR chondrites on average have exposure ages around 8 Ma and range from 1 to 25 Ma (e.g. Herzog and Caffee, 2014). The CRE age of Jbilet Winselwan is also missing, but other CM chondrites have published exposure ages of up to 6.5 Ma (Eugster et al., 1998). Considering our Cd isotope data, these expected age ranges for EET 92048, MIL 090001 and Jbilet Winselwan seem realistic. Based on the available CRE ages of our analysed samples, Indarch should show the largest neutron capture induced shift in ε^{113}Cd, followed by Allende. Murchison, with the shortest exposure age, should display the smallest effects. This fits our data quite well (Fig. S3), considering that the shielding depth and meteorite radius also influence the neutron capture effect.

Leya and Masarik (2013) modelled the expected Cd isotope variations in carbonaceous chondrites produced by neutron capture for samples of different exposure ages, meteorite radius (10–500 cm) and shielding depth. The pre-atmospheric radius of some of the analysed meteorites are known and thus can be used to cross-check our results with the predicted values. Allende has an estimated radius of at least 50 cm (e.g. Cressy, 1972) and Murchison of 35 cm (Roth et al., 2011). Using the model of Leya and Masarik (2013), a 4.8 ± 0.5 Ma CRE age and a radius of 50 cm yields ε^{113}Cd values between −0.19 and −2.98, depending on the shielding depth. This fits our Allende data with −0.36 ± 0.27 for ε^{113}Cd, if our sample originates from very shallow depths of 0–4 cm. As for Murchison, a 1.6 ± 0.3 Ma exposure age and a radius of 35 cm results in an ε^{113}Cd offset between −0.05 and −0.83, again depending on shielding depth. This also fits our data for Murchison of −0.23 ± 0.27 for ε^{113}Cd at depths of 0–20 cm. The match between our results and the Leya and Masarik (2013) model for Murchison are very good. However, the depths predicted for Allende appear too shallow. Possible reasons for this discrepancy include: (i) a significantly larger (≥300 cm) pre-atmospheric radius of Allende than estimated, which would provide a match with our Cd isotope data at much greater depths, (ii) neutron capture induced Cd isotope shifts that are overestimated by the model of Leya and Masarik (2013), or (iii) a combination of both. Such discrepancy between the model and real samples were observed previously, e.g. for Pt (Hunt et al., 2017).

Our Cd isotope data provides evidence that ^{113}Cd starts to display resolvable negative shifts for chondrites with exposure ages of a few Ma (Table 2, Fig. 1). This is the first study to demonstrate that Cd isotopes can show resolvable neutron-capture induced effects in bulk carbonaceous and enstatite chondrites. Our new results imply that Cd might be an ideal thermal neutron capture monitor for stony meteorites with enough Cd for high-precision isotope analysis (~100 ng Cd separated for analysis). Because Cd isotopes show no resolvable nucleosynthetic variations and since there is no need to obtain precise elemental concentrations (as e.g. of Ir for some applications of Pt isotopes as a neutron-dose proxy (e.g. Hunt et al., 2017)), Cd is well-suited to constrain the exposure histories of samples poor in platinum group elements (PGE's), where other neutron-dose proxies (e.g. Pt, Os) cannot be applied.

Furthermore, our Cd data indicates that thermal neutron capture effects can potentially be resolved and should not be disregarded in primitive chondrites when assessing nucleosynthetic isotope variations. It is important to note that ^{113}Cd has a very large neutron-capture cross-section (~20,000 barns) and other elements with smaller cross-sections, such as Os, show no evidence for neutron-capture induced effects in bulk carbonaceous chondrites (Goderis et al., 2017). Molybdenum, Ru and Zr isotopes have even smaller neutron-capture cross-sections than Os. For Zr, Leya et al. (2003) modelled the potential effect of neutron capture effects on the ^{92}Zr/^{90}Zr ratio and found them to be irrelevant even when assuming an exposure age of ~100 Ma, which is well in excess of typical carbonaceous chondrites. Therefore, neutron-capture effects in carbonaceous chondrites that could potentially influence the mass-independent nucleosynthetic isotope variations of Zr, Ru and Mo in chondrites are unlikely (e.g. Zr, (Akram et al., 2015), Ru (Fischer-Gödde et al., 2015) and Mo (Burkhardt et al., 2011)) based on current data and models. However, with improved analytical precision it will become increasingly important to address all possible sources of mass-independent isotope variations when interpreting the results.

5. CONCLUSIONS

High-precision bulk rock data of carbonaceous and enstatite chondrites do not display resolvable nucleosynthetic Cd isotope variations. The seven leachate fractions of Jbilet Winselwan agree with the bulk chondrite isotope data and show that Cd is extremely depleted in the more refractory, acid-resistant phases. The hotplate and bomb digested samples of Allende yield identical compositions within uncertainty, further indicating that no refractory phases with significant anomalous Cd are present. The CR2 chondrite GRA 06100 is particular because it is highly depleted in Cd and therefore analytical uncertainties are large. It displays potential Cd isotope variations at a bulk rock scale that hint at an *s*-process deficit/*r*-process excess in combination with cosmogenic effects. Overall, the nucleosynthetic homogeneity of Cd isotopes in chondrites and their components is in good agreement with findings from other moderately volatile elements. We propose that the isotopic homogenisation of Cd nucleosynthetic diversity is, in part, due to incomplete condensation into dust in the stellar formation environment. Further mixing and homogenisation occurred in the solar nebula through thermal processing and on the parent body due to aqueous alteration and thermal metamorphism.

All high-precision Cd isotope data of bulk chondrites, except for Murchison and EET 92048, show small but resolvable negative ε^{113}Cd ranging from −0.30 ± 0.18 to −0.56 ± 0.27. Jbilet Winselwan also exhibits a small positive ε^{114}Cd offset of +0.29 ± 0.24. These Cd isotope varia-

tions likely represent neutron-capture induced shifts that are due to the very large thermal neutron-capture cross-section of ^{113}Cd. This renders Cd a potential candidate as a thermal neutron capture monitor, in addition to Sm and Gd.

Declaration of Competing Interest

The authors declare that they have no known competing financial interests or personal relationships that could have appeared to influence the work reported in this paper.

ACKNOWLEDGEMENTS

We thank the ANSMET program for the provision of the analysed CR chondrites (MIL 090001, EET 92048 and GRA 06100). US Antarctic meteorite samples are recovered by the Antarctic Search for Meteorites (ANSMET) program which has been funded by NSF and NASA, and characterized and curated by the Department of Mineral Sciences of the Smithsonian Institution and Astromaterials Acquisition and Curation Office at NASA Johnson Space Center. We also wish to thank Philipp Heck from the Field Museum of Natural History in Chicago for providing us with samples of Indarch (ME 1403) and Murchison (ME 2752). Adrian Gilli is thanked for providing the sediment sample of Lake Zürich. Martin Schiller, Andrew M. Davis and an anonymous reviewer are thanked for their constructive reviews. This work has been financially supported by ETH Zürich. It has been partially carried out within the framework of the National Centre for Competence in Research PlanetS supported by the Swiss National Science Foundation. Matthias Friebel was supported by the Swiss National Science Foundation (Project 200021_149282).

APPENDIX A. SUPPLEMENTARY MATERIAL

Supplementary data to this article can be found online at https://doi.org/10.1016/j.gca.2020.01.059.

REFERENCES

Abreu N. M. and Bullock E. S. (2013) Opaque assemblages in CR2 Graves Nunataks (GRA) 06100 as indicators of shock-driven hydrothermal alteration in the CR chondrite parent body. *Meteorit. Planet. Sci.* **48**, 2406–2429.

Akram W., Schönbächler M., Bisterzo S. and Gallino R. (2015) Zirconium isotope evidence for the heterogeneous distribution of s-process materials in the solar system. *Geochim. Cosmochim. Acta* **165**, 484–500.

Akram W., Schönbächler M., Sprung P. and Vogel N. (2013) Zirconium-Hafnium isotope evidence from meteorites for the decoupled synthesis of light and heavy neutron-rich nuclei. *Astrophys. J.* **777**, 169–180.

Andreasen R. and Sharma M. (2006) Solar nebula heterogeneity in p-process samarium and neodymium isotopes. *Science* **314**, 806–809.

Andreasen R. and Sharma M. (2007) Mixing and homogenization in the early solar system: clues from Sr, Ba, Nd, and Sm isotopes in meteorites. *Astrophys. J.* **665**, 874–883.

Baker R. G. A., Schönbächler M., Rehkämper M., Williams H. M. and Halliday A. N. (2010) The thallium isotope composition of carbonaceous chondrites - New evidence for live ^{205}Pb in the early solar system. *Earth Planet. Sci. Lett.* **291**, 39–47.

Bisterzo S., Gallino R., Straniero O., Cristallo S. and Käppeler F. (2011) The s-process in low-metallicity stars – II. Interpretation of high-resolution spectroscopic observations with asymptotic giant branch models. *Mon. Not. R. Astron. Soc.* **418**, 284–319.

Bouvier A. and Boyet M. (2016) Primitive Solar System materials and Earth share a common initial ^{142}Nd abundance. *Nature* **537**, 399–402.

Briani G., Quirico E., Gounelle M., Paulhiac-Pison M., Montagnac G., Beck P., Orthous-Daunay F.-R., Bonal L., Jacquet E., Kearsley A. and Russell S. S. (2013) Short duration thermal metamorphism in CR chondrites. *Geochim. Cosmochim. Acta* **122**, 267–279.

Burkhardt C., Borg L. E., Brennecka G. A., Shollenberger Q. R., Dauphas N. and Kleine T. (2016) A nucleosynthetic origin for the Earth's anomalous ^{142}Nd composition. *Nature* **537**, 394–398.

Burkhardt C., Kleine T., Oberli F., Pack A., Bourdon B. and Wieler R. (2011) Molybdenum isotope anomalies in meteorites: Constraints on solar nebula evolution and origin of the Earth. *Earth Planet. Sci. Lett.* **312**, 390–400.

Carlson R. W., Boyet M. and Horan M. (2007) Chondrite barium, neodymium, and samarium isotopic heterogeneity and early Earth differentiation. *Science* **316**, 1175–1178.

Chen H.-W., Lee T., Lee D.-C., Shen J. J.-S. and Chen J.-C. (2011) ^{48}Ca heterogeneity in differentiated meteorites. *Astrophys. J. Lett.* **743**, L23–L27.

Chen J. H., Papanastassiou D. A. and Wasserburg G. J. (2010) Ruthenium endemic isotope effects in chondrites and differentiated meteorites. *Geochim. Cosmochim. Acta* **74**, 3851–3862.

Cressy, Jr., P. J. (1972) Cosmogenic radionuclides in the Allende and Murchison carbonaceous chondrites. *J. Geophys. Res.* **77**, 4905–4911.

Dauphas N., Chen J. H., Zhang J., Papanastassiou D. A., Davis A. M. and Travaglio C. (2014) Calcium-48 isotopic anomalies in bulk chondrites and achondrites: Evidence for a uniform isotopic reservoir in the inner protoplanetary disk. *Earth Planet. Sci. Lett.* **407**, 96–108.

Dauphas N., Davis A. M., Marty B. and Reisberg L. (2004) The cosmic molybdenum-ruthenium isotope correlation. *Earth Planet. Sci. Lett.* **226**, 465–475.

Dauphas N., Remusat L., Chen J. H., Roskosz M., Papanastassiou D. A., Stodolna J., Guan Y., Ma C. and Eiler J. M. (2010) Neutron-rich chromium isotope anomalies in supernova nanoparticles. *Astrophys. J.* **720**, 1577–1591.

Ek M., Hunt A. C., Lugaro M. and Schönbächler M. (2020) The origin of s-process isotope heterogeneity in the solar protoplanetary disk. *Nat. Astron.*. https://doi.org/10.1038/s41550-019-0948-z.

Eugster O., Eberhardt P., Thalmann Ch. and Weigel A. (1998) Neon-E in CM-2 chondrite LEW90500 and collisional history of CM-2 chondrites, Maralinga, and other CK chondrites. *Geochim. Cosmochim. Acta* **62**, 2573–2582.

Eugster O., Lorenzetti S., Krähenbühl U. and Marti K. (2007) Comparison of cosmic-ray exposure ages and trapped noble gases in chondrule and matrix samples of ordinary, enstatite, and carbonaceous chondrites. *Meteorit. Planet. Sci.* **42**, 1351–1371.

Eugster O., Tera F., Burnett D. S. and Wasserburg G. J. (1970) Neutron capture effects in Gd from the Norton County meteorite. *Earth Planet. Sci. Lett.* **7**, 436–440.

Fehr M. A., Rehkämper M., Halliday A. N. and Schönbächler M. (2006) Search for nucleosynthetic and radiogenic tellurium isotope anomalies in carbonaceous chondrites. *Geochim. Cosmochim. Acta* **70**, 3436–3448.

Fehr M. A., Rehkämper M., Halliday A. N., Wiechert U., Hattendorf B., Günther D., Ono S., Eigenbrode J. L. and

Rumble (2005) Tellurium isotopic composition of the early solar system—A search for effects resulting from stellar nucleosynthesis, ^{126}Sn decay, and mass-independent fractionation. *Geochim. Cosmochim. Acta* **69**, 5099–5112.

Fischer-Gödde M., Burkhardt C., Kruijer T. S. and Kleine T. (2015) Ru isotope heterogeneity in the solar protoplanetary disk. *Geochim. Cosmochim. Acta* **168**, 151–171.

Friebel M. (2018) *Tin stable isotope cosmochemistry* PhD thesis. ETH Zürich.

Friebel M., Toth E. R., Fehr M. A. and Schönbächler M. (2020) Efficient separation and high-precision analyses of tin and cadmium isotopes in geological materials. *J. Anal. At. Spectrom.* **35**, 273–292. https://doi.org/10.1039/c9ja00289h.

Friedrich J. M., Abreu N. M., Wolf S. F., Troiano J. M. and Stanek G. L. (2018) Redox-influenced trace element compositional differences among variably aqueously altered CM chondrites. *Geochim. Cosmochim. Acta* **237**, 1–17.

Fukami Y. and Yokoyama T. (2017) Tellurium isotope compositions in acid leach fractions of carbonaceous chondrites. *Geochem. J.* **51**, 17–29.

Gault-Ringold M. and Stirling C. H. (2012) Anomalous isotopic shifts associated with organic resin residues during cadmium isotopic analysis by double spike MC-ICPMS. *J. Anal. At. Spectrom.* **27**, 449–459.

Goderis S., Brandon A. D., Mayer B. and Humayun M. (2017) Osmium isotopic homogeneity in the CK carbonaceous chondrites. *Geochim. Cosmochim. Acta* **216**, 8–27.

Goderis S., Brandon A. D., Mayer B. and Humayun M. (2015) s-Process Os isotope enrichment in ureilites by planetary processing. *Earth Planet. Sci. Lett.* **431**, 110–118.

Herzog G. F. and Caffee M. W. (2014) Cosmic-ray exposure ages of meteorites. In Meteorites and Cosmochemical Processes (Ed. A. M. Davis), Vol. 1 Treatise on Geochemistry, 2nd Ed. (Exec. Eds. H. D. Holland and K. K. Turekian), Elsevier, Oxford, pp. 419–453.

Hidaka H., Ebihara M. and Yoneda S. (2000) Isotopic study of neutron capture effects on Sm and Gd in chondrites. *Earth Planet. Sci. Lett.* **180**, 29–37.

Horner T. J., Schönbächler M., Rehkämper M., Nielsen S. G., Williams H., Halliday A. N., Xue Z. and Hein J. R. (2010) Ferromanganese crusts as archives of deep water Cd isotope compositions. *Geochem. Geophys. Geosyst.* **11**, 1–10.

Hunt A. C., Cook D. L., Lichtenberg T., Reger P. M., Ek M., Golabek G. J. and Schönbächler M. (2018) Late metal–silicate separation on the IAB parent asteroid: constraints from combined W and Pt isotopes and thermal modelling. *Earth Planet. Sci. Lett.* **482**, 490–500.

Hunt A. C., Ek M. and Schönbächler M. (2017) Platinum isotopes in iron meteorites: galactic cosmic ray effects and nucleosynthetic homogeneity in the p-process isotope ^{190}Pt and the other platinum isotopes. *Geochim. Cosmochim. Acta* **216**, 82–95.

King A. J., Russell S. S., Schofield P. F., Humphreys-Williams E. R., Strekopytov S., Abernethy F. A. J., Verchovsky A. B. and Grady M. M. (2019) The alteration history of the Jbilet Winselwan CM carbonaceous chondrite: an analog for C-type asteroid sample return. *Meteorit. Planet. Sci.* **54**, 521–543.

Van Kooten E. M. M. E., Wielandt D., Schiller M., Nagashima K., Thomen A., Larsen K. K., Olsen M. B., Nordlund Å., Krot A. N. and Bizzarro M. (2016) Isotopic evidence for primordial molecular cloud material in metal-rich carbonaceous chondrites. *Proc. Natl. Acad. Sci.* **113**, 2011–2016.

Kruijer T. S., Sprung P., Kleine T., Leya I. and Wieler R. (2013) The abundance and isotopic composition of Cd in iron meteorites. *Meteorit. Planet. Sci.* **48**, 2597–2607.

Labidi J., König S., Kurzawa T., Yierpan A. and Schoenberg R. (2018) The selenium isotopic variations in chondrites are mass-dependent; implications for sulfide formation in the early solar system. *Earth Planet. Sci. Lett.* **481**, 212–222.

Leya I. and Masarik J. (2013) Thermal neutron capture effects in radioactive and stable nuclide systems. *Meteorit. Planet. Sci.* **48**, 665–685.

Leya I., Schönbächler M., Wiechert U., Krähenbühl U. and Halliday A. N. (2008) Titanium isotopes and the radial heterogeneity of the solar system. *Earth Planet. Sci. Lett.* **266**, 233–244.

Leya I., Wieler R. and Halliday A. N. (2003) The influence of cosmic-ray production on extinct nuclide systems. *Geochim. Cosmochim. Acta* **67**, 529–541.

Lodders K. (2003) Solar system abundances and condensation temperatures of the elements. *Astrophys. J.* **591**, 1220–1247.

Lodders K. and Fegley, Jr., B. (1997) Complementary trace element abundances in meteoritic SiC grains and carbon star atmospheres. *Astrophys. J.* **484**, L71–L74.

Maas R., Loss R. D., Rosman K. J. R., De Laeter J. R., Lewis R. S., Huss G. R. and Lugmair G. W. (2001) Isotope anomalies in tellurium and palladium from Allende nanodiamonds. *Meteorit. Planet. Sci.* **36**, 849–858.

Mahan B., Moynier F., Beck P., Pringle E. A. and Siebert J. (2018) A history of violence: insights into post-accretionary heating in carbonaceous chondrites from volatile element abundances, Zn isotopes and water contents. *Geochim. Cosmochim. Acta* **220**, 19–35.

Masarik J. (1997) Contribution of neutron-capture reactions to observed tungsten isotopic ratios. *Earth Planet. Sci. Lett.* **152**, 181–185.

Moynier F., Dauphas N. and Podosek F. A. (2009) A search for ^{70}Zn anomalies in meteorites. *Astrophys. J.* **700**, L92–L95.

Murphy K., Rehkämper M., Kreissig K., Coles B. and van de Flierdt T. (2016) Improvements in Cd stable isotope analysis achieved through use of liquid-liquid extraction to remove organic residues from Cd separates obtained by extraction chromatography. *J. Anal. At. Spectrom.* **31**, 319–327.

Nanne J. A. M., Nimmo F., Cuzzi J. N. and Kleine T. (2019) Origin of the non-carbonaceous–carbonaceous meteorite dichotomy. *Earth Planet. Sci. Lett.* **511**, 44–54.

Palme H., Lodders K. and Jones A. (2014) Solar system abundances of the elements. In Planets, Asteroids, Comets and The Solar System (Ed. A. M. Davis), Vol. 2 Treatise on Geochemistry, 2nd Ed. (Exec. Eds. H. D. Holland and K. K. Turekian), Elsevier, Oxford, pp. 15–36.

Poole G. M., Rehkämper M., Coles B. J., Goldberg T. and Smith C. L. (2017) Nucleosynthetic molybdenum isotope anomalies in iron meteorites – new evidence for thermal processing of solar nebula material. *Earth Planet. Sci. Lett.* **473**, 215–226.

Qin L., Alexander C. M. O., Carlson R. W., Horan M. F. and Yokoyama T. (2010) Contributors to chromium isotope variation of meteorites. *Geochim. Cosmochim. Acta* **74**, 1122–1145.

Regelous M., Elliott T. and Coath C. D. (2008) Nickel isotope heterogeneity in the early Solar System. *Earth Planet. Sci. Lett.* **272**, 330–338.

Richter S., Ott U. and Begemann F. (1998) Tellurium in pre-solar diamonds as an indicator for rapid separation of supernova ejecta. *Nature* **391**, 261–263.

Rotaru M., Birck J. L. and Allègre C. J. (1992) Clues to early Solar System history from chromium isotopes in carbonaceous chondrites. *Nature* **358**, 465–470.

Roth A. S. G., Baur H., Heber V. S., Reusser E. and Wieler R. (2011) Cosmogenic helium and neon in individual chondrules from Allende and Murchison: implications for the precompaction exposure history of chondrules. *Meteorit. Planet. Sci.* **46**, 989–1006.

Sands D. G., De Laeter J. R. and Rosman K. J. R. (2001) Measurements of neutron capture effects on Cd, Sm and Gd in lunar samples with implications for the neutron energy spectrum. *Earth Planet. Sci. Lett.* **186**, 335–346.

Schiller M., Paton C. and Bizzarro M. (2015) Evidence for nucleosynthetic enrichment of the protosolar molecular cloud core by multiple supernova events. *Geochim. Cosmochim. Acta* **149**, 88–102.

Schönbächler M., Carlson R. W., Horan M. F., Mock T. D. and Hauri E. H. (2008) Silver isotope variations in chondrites: Volatile depletion and the initial ^{107}Pd abundance of the solar system. *Geochim. Cosmochim. Acta* **72**, 5330–5341.

Schönbächler M., Lee D.-C., Rehkämper M., Halliday A. N., Fehr M. A., Hattendorf B. and Günther D. (2003) Zirconium isotope evidence for incomplete admixing of r-process components in the solar nebula. *Earth Planet. Sci. Lett.* **216**, 467–481.

Schönbächler M., Rehkämper M., Fehr M. A., Halliday A. N., Hattendorf B. and Günther D. (2005) Nucleosynthetic zirconium isotope anomalies in acid leachates of carbonaceous chondrites. *Geochim. Cosmochim. Acta* **69**, 5113–5122.

Sprung P., Scherer E. E., Upadhyay D., Leya I. and Mezger K. (2010) Non-nucleosynthetic heterogeneity in non-radiogenic stable Hf isotopes: implications for early solar system chronology. *Earth Planet. Sci. Lett.* **295**, 1–11.

Steele R. C. J., Coath C. D., Regelous M., Russell S. and Elliott T. (2012) Neutron-poor nickel isotope anomalies in meteorites. *Astrophys. J.* **758**, 59–80.

Trinquier A., Birck J. and Allègre C. J. (2007) Widespread ^{54}Cr heterogeneity in the inner solar system. *Astrophys. J.* **655**, 1179–1185.

Trinquier A., Elliott T., Ulfbeck D., Coath C., Krot A. N. and Bizzarro M. (2009) Origin of nucleosynthetic isotope heterogeneity in the solar protoplanetary disk. *Science* **324**, 374–376.

Wittig N., Humayun M., Brandon A. D., Huang S. and Leya I. (2013) Coupled W-Os-Pt isotope systematics in IVB iron meteorites: In situ neutron dosimetry for W isotope chronology. *Earth Planet. Sci. Lett.* **361**, 152–161.

Wombacher F., Rehkämper M. and Mezger K. (2004) Determination of the mass-dependence of cadmium isotope fractionation during evaporation. *Geochim. Cosmochim. Acta* **68**, 2349–2357.

Wombacher F., Rehkämper M., Mezger K., Bischoff A. and Münker C. (2008) Cadmium stable isotope cosmochemistry. *Geochim. Cosmochim. Acta* **72**, 646–667.

Wombacher F., Rehkämper M., Mezger K. and Münker C. (2003) Stable isotope compositions of cadmium in geological materials and meteorites determined by multiple-collector ICPMS. *Geochim. Cosmochim. Acta* **67**, 4639–4654.

Wood B. J., Smythe D. J. and Harrison T. (2019) The condensation temperatures of the elements: a reappraisal. *Am. Mineral.* **104**, 844–856.

Yokoyama T., Alexander C. M. O. and Walker R. J. (2010) Osmium isotope anomalies in chondrites: results for acid residues and related leachates. *Earth Planet. Sci. Lett.* **291**, 48–59.

Zhang J., Dauphas N., Davis A. M., Leya I. and Fedkin A. (2012) The proto-Earth as a significant source of lunar material. *Nat. Geosci.* **5**, 251–255.

Zinner E. (2014) Presolar Grains. In Meteorites and Cosmochemical Processes (Ed. A. M. Davis), Vol. 1 Treatise on Geochemistry, 2nd Ed. (Exec. Eds. H. D. Holland and K. K. Turekian), Elsevier, Oxford, pp. 181–213.

Associate editor: Frederic Moynier